ARTICLE

Recyclable rhodium catalyst anchored onto bipyridine covalent triazine framework for transfer hydrogenation of N-heteroarenes in water

Jonas Everaert,[a] Karen Leus,[b] Hannes Rijckaert,[c] Maarten Debruyne,[a] Kristof Van Hecke,[c] Rino Morent,[b] Nathalie De Geyter,[b] Veronique Van Speybroeck,[d] Pascal Van Der Voort,[c] Christian V. Stevens*[a]

Covalent triazine frameworks (CTFs) based on polydentate ligands are highly promising supports to coordinate well-defined active metal complexes, hereby combining the well-known reactivity of homogeneous catalysts with the robustness and recyclability of heterogeneous catalysts. Herein, we describe the immobilization of a half-sandwich Rh(III) complex onto a bipyridine-based CTF and its application for the transfer hydrogenation of N-heteroarenes in water with benign sodium formate as the hydrogen source. The heterogenized catalyst exhibited excellent activity toward a wide variety of quinoxalines and various other N-heteroarenes. Moreover, the catalyst maintained high activity during recycling and could be implemented in a continuous flow synthesis.

Introduction

1,2,3,4-Tetrahydroquinoxalines and analogous N-heterocycles are prominent structural motifs in bioactive natural products,[1] pharmaceuticals[2-7] and agrochemicals.[8] In the process of drug design, these saturated N-heterocycles serve as important building blocks for potential drug candidates with increased three-dimensionality, thereby 'escaping from flatland' and exploring a larger chemical space.[9,10] Consequently, the synthesis of partially saturated N-heterocycles has attracted widespread attention. The most straightforward route to these scaffolds is the regioselective hydrogenation of the parent azaarene. Although catalytic hydrogenation with molecular hydrogen gas is a very atom-efficient strategy, high pressures and temperatures are generally required to break the aromaticity in the substrates.[11-13] Hence, specialized reaction equipment and safety procedures must be in place for handling and storing of the highly flammable hydrogen gas. As an alternative, catalytic transfer hydrogenation with H_2-surrogates, such as isopropanol or formic acid, offers a mild yet powerful method due to its operational simplicity and the widespread availability of suitable reducing agents.[14,15] The catalysts of choice to assist in the hydrogen transfer are typically half-sandwich complexes of the precious metals Ru, Rh and Ir due to their superior catalytic activities.[14] In particular, their performance in aqueous media using formate as hydrogen donor has been extensively studied over the past two decades.[16-19] In addition to the environmentally benign aspects of water as a solvent, it has been reported that transfer hydrogenation proceeds much faster in water than in organic solvents.[20-23] However, due to the homogeneous nature of these metal complexes, their separation from the product and recycling are difficult to achieve. These obstacles direct the use of heterogeneous catalytic systems for more sustainable processes, especially when it comes to catalysts based on precious and toxic transition metals.

The immobilization of the well-defined metal complexes on a solid porous support is an attractive strategy to overcome the aforementioned obstacles while maintaining the high activity and selectivity of the homogeneous catalyst. Moreover, the heterogenization facilitates the application of the catalyst in continuous flow chemistry, which is currently gaining momentum in the fine chemical and pharmaceutical industry. In this context, covalent triazine frameworks (CTFs) have recently emerged as promising solid supports for the immobilization of active metal species.[24-27] These nanoporous polymeric materials are constructed from organic building blocks that are covalently connected through triazine units which provide the framework with superior thermal and chemical stability.[28,29] The modular design of CTFs allows the porosity, pore size, specific surface area and the surface functionality to be tailored to the chosen application. In

a. SynBioC Research Group, Department of Green Chemistry and Technology, Faculty of Bioscience Engineering, Ghent University, Coupure Links 653, B-9000 Ghent, Belgium. E-mail: Chris.Stevens@UGent.be
b. Department of Applied Physics, Faculty of Engineering and Architecture, Ghent University, Sint-Pietersnieuwstraat 41-B4, B-9000 Ghent, Belgium.
c. Department of Chemistry, Faculty of Sciences, Ghent University, Krijgslaan 281-S3, B-9000 Ghent, Belgium.
d. Center for Molecular Modeling (CMM), Ghent University, Technologiepark 46, B-9052 Zwijnaarde, Belgium.

addition, the diversity of these frameworks is beyond limits thanks to an ever-expanding and versatile set of available building blocks.

CTFs based on 2,2'-bipyridine building blocks possess strong bipyridine-binding sites.[30-35] Hence, we considered the heterogenization of a well-defined metal complex on a bipyridine-based CTF (bpyCTF), allowing the preservation of its coordination environment and catalytic activity. Recently, the homogeneous [Cp*Rh(bpy)Cl]Cl complex (Cp* = η^5-C_5Me_5) has been identified as an effective catalyst for the transfer hydrogenation of various N-heteroarenes.[36] Herein, we describe the synthesis of a bpyCTF-supported Cp*Rh catalyst and its application for the transfer hydrogenation of N-heteroarenes in water using sodium formate as the hydrogen donor. The broad applicability of the heterogenized catalyst was demonstrated by the efficient hydrogenation of a wide range of quinoxalines and other N-heteroarenes. The high stability of the catalyst allowed its easy separation and reuse, and the catalyst could be implemented in a packed-bed reactor to explore its performance in the continuous flow transfer hydrogenation.

Results and discussion

Catalyst preparation and characterization

The bipyridine-based CTF (bpyCTF) was prepared from 2,2'-bipyridine-5,5'-dicarbonitrile **1**, which was accessed through a Ni-catalyzed reductive homocoupling of 2-bromo-5-cyanopyridine.[37,38] The homocoupling proceeded efficiently at a mild temperature and without the necessity of an external ligand since the coupling product could serve as a ligand itself. The monomers were then polymerized using the classical ionothermal CTF-synthesis method (Schema 1).[30] To this end, bipyridine **1** and $ZnCl_2$, which acted both as the solvent and as a the Lewis acid catalyst to promote trimerization, were heated together in a sealed ampule at 400 °C for 48 h. Treatment of the

obtained CTF with water and 1 M aqueous HCl solution to remove the remaining $ZnCl_2$ and extensive washing with organic solvents afforded bpyCTF as a glassy black powder.

The completion of the trimerization was confirmed by comparison of the Fourier transform infrared (FT-IR) spectra of bpyCTF and bipyridine **1** (Figure S1, ESI). The distinctive C≡N stretching band at 2239 cm^{-1} disappeared in the spectrum of bpyCTF, whereas the characteristic stretching bands for triazine at 1513 and 1348 cm^{-1} were present.[30,39] However, the measured spectrum showed only broad absorption bands, indicating that the formed CTF deviated from the idealized framework structure. In addition, elemental analysis of bpyCTF revealed an increased C/N molar ratio of 5.1 compared to the theoretical ratio of 3.0, evidencing the occurrence of partial carbonization of the framework during the synthesis reaction, as is well known for CTFs synthesized under the harsh ionothermal conditions (Table S1, ESI).[28,40] The powder X-ray diffraction (PXRD) pattern of bpyCTF featured a broad diffraction peak centered at 2θ = 26° and is ascribed to (001) reflection, indicating short-range "graphitic" layer stacking (Figure S2, ESI).[30] From the 2θ angle, an idealized interlayer distance of 3.5 Å was derived using Bragg's law. However, the broadness of the diffraction peak indicated the limited long-range order of the material, which is the result of the harsh ionothermal conditions.

The numerous bipyridine motifs in bpyCTF constitute excellent anchoring sites for metal complexes. Hence, Rh@bpyCTF was readily prepared in a post-synthetic metalation approach using [Cp*RhCl$_2$]$_2$ as catalyst precursor (Scheme 1). The metal complex was employed in a Rh/bpy ratio of 5 mol% or 0.24 mmol g^{-1} (2.5 wt%). To our delight, nearly all the added catalyst precursor was grafted to bpyCTF as indicated by an actual Rh loading of 4.6 mol% or 0.22 mmol g^{-1} (2.3 wt%), measured by inductively coupled plasma-optical emission spectrometry (ICP-OES). The close approximation of the actual Rh content to the target content demonstrates that the
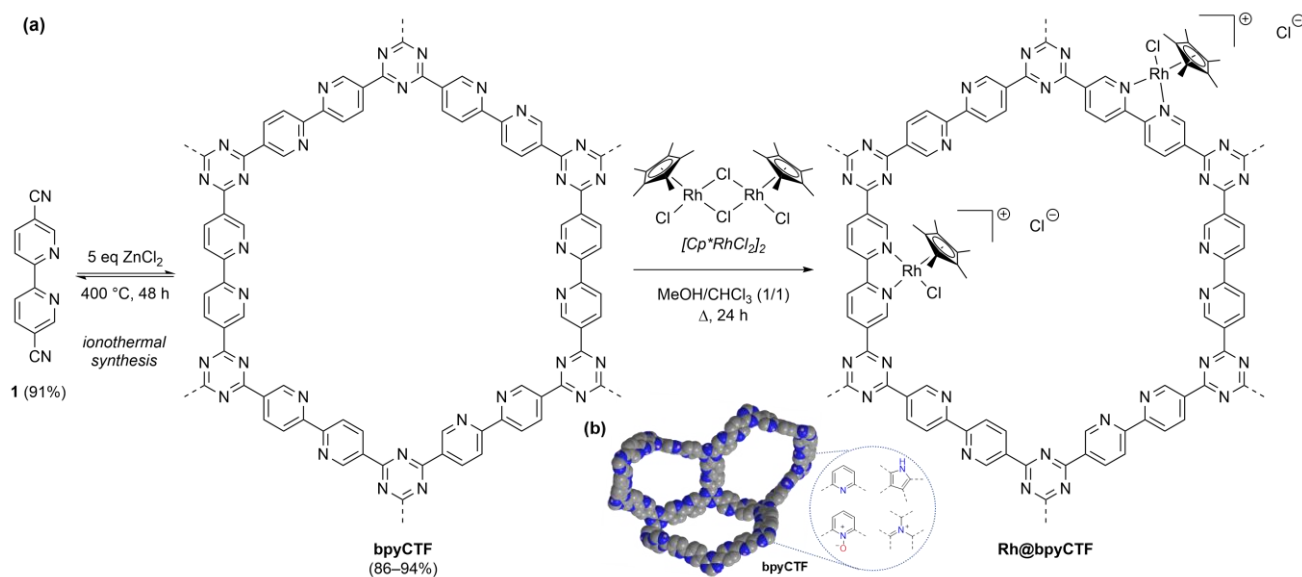
Scheme 1. (a) Preparation of Rh@bpyCTF by ionothermal synthesis of bpyCTF and post-synthetic metalation with [Cp*RhCl$_2$]$_2$. The drawn structure of bpyCTF is an idealized representation without defects. (b) Schematic illustration of the possible structure of bpyCTF after synthesis under ionothermal conditions.
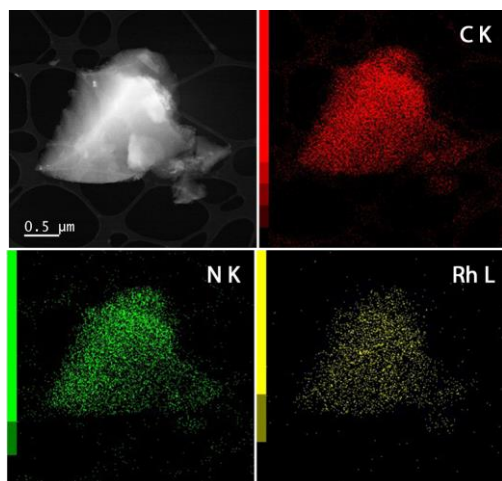
Figure 1. HAADF-STEM image of Rh@bpyCTF with corresponding EDX elemental mapping of carbon, nitrogen, and rhodium.

rhodium loading can be easily modulated by the added amount of catalyst precursor. The presence of Rh was further confirmed by combined scanning transmission electron microscopy (STEM) and energy-dispersive X-ray (EDX) spectroscopy, showing a homogeneous distribution of the Rh atoms within the framework (Figure 1).

The permanent porosity of bpyCTF and Rh@bpyCTF was assessed by N_2 sorption measurements at 77 K (Figure 2a). Both CTFs displayed isotherms that feature a steep rise at low relative pressures (P/P$_0$ < 0.03), after which they quickly reached a plateau. Following the IUPAC classification, the isotherms clearly represent a Type I isotherm, which is typically given by purely microporous materials.[41] The calculated Brunauer–Emmett–Teller (BET) specific surface area for bpyCTF was 671 m^2 g^{-1} and is comparable to values obtained in the literature.[35,42] Furthermore, bpyCTF had a total pore volume of 0.27 cm^3 g^{-1} and a narrow pore size distribution centered at 1.67 nm, highlighting its microporosity (Figure S3, ESI). Upon metalation with the Rh complex, the BET specific surface area decreased to 408 m^2 g^{-1} and the total pore volume to 0.22 cm^3 g^{-1}, suggesting the partial occupation of the pores by anchored metal complex. Nonetheless, Rh@bpyCTF still exhibited abundant porosity, ensuring accessibility of the catalytic sites.

A deeper understanding of the chemical bonding states of the elements present in the CTFs was provided by X-ray photoelectron spectroscopy (XPS). The high-resolution C 1s spectrum of Rh@bpyCTF, depicted in Figure 2b, remained similar to that of pristine bpyCTF (Figure S4, ESI) and showed two main peaks located at 284.9 and 285.7 eV, corresponding to aromatic (C=C) and bipyridine/triazine (C=N) carbon atoms, respectively.[43] The weak contributions at 288.0 and 288.9 eV indicated the minor presence of the surface oxygen species C=O and O–C=O, respectively. The binding states of nitrogen in bpyCTF were analyzed in the high-resolution N 1s XPS spectrum (Figure 2c). In the curve fitting, contributions of four types of
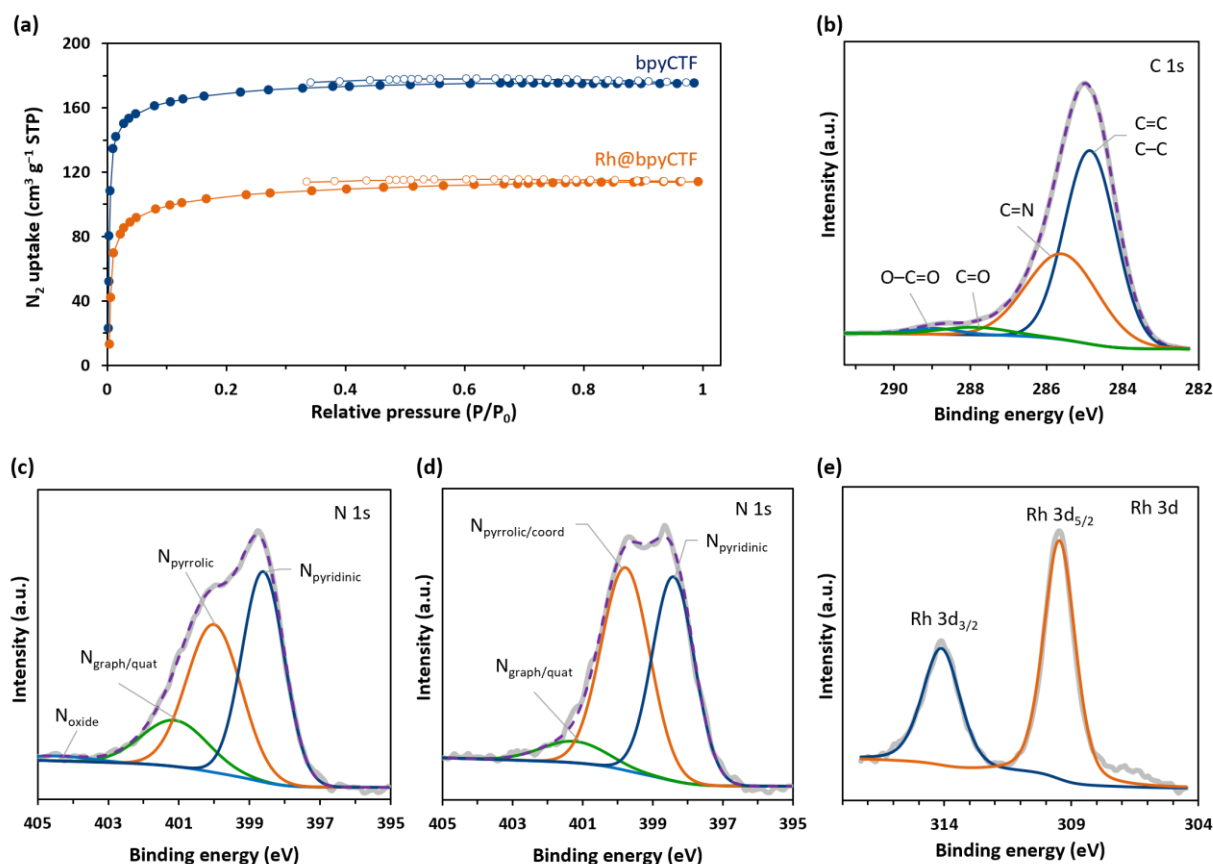

Figure 2. (a) Nitrogen adsorption (●) and desorption (○) isotherms of bpyCTF and Rh@bpyCTF at 77 K. (b) High-resolution C 1s XPS spectrum and (e) Rh 3d XPS spectrum of Rh@bpyCTF. High-resolution N 1s XPS spectra of (c) bpyCTF and (d) Rh@bpyCTF.

nitrogen species could be distinguished. A dominant peak appeared at 398.6 eV, associated with pyridinic N from the bipyridine and triazine units.[40,44,45] The signals at 400.0 and 401.2 eV are assigned to pyrrolic N and graphitic/quaternary N species, respectively. The presence of these N species confirms the occurrence of decomposition reactions during the ionothermal synthesis. A broad, almost negligible peak at 404.6 eV can be assigned to pyridinic N-oxide species presumably formed by contact with air after the synthesis. The N 1s spectrum of Rh@bpyCTF displayed an increased relative intensity at 400.0 eV, originating from the coordination of bipyridine-derived pyridinic N with Rh (Figure 2d). As the Rh metal center withdraws valence electron density from the pyridinic N species, the core electrons of N bind stronger to the nucleus, causing a shift of pyridinic N-contribution toward higher binding energies. A similar shift was observed by Soorholtz *et al.* for a pyridine CTF coordinated with Pt.[46] In the Rh 3d XPS spectrum of Rh@bpyCTF (Figure 2e), the peaks observed at binding energies 309.5 and 314.2 eV are characteristic for the Rh $3d_{5/2}$ and $3d_{3/2}$ core levels, respectively, and correspond to a +3 oxidation state.[47] The $3d_{5/2}$ peak observed for Rh@bpyCTF is shifted to a substantially higher binding energy compared to the Rh $3d_{5/2}$ peak at 308.3 eV reported for the employed catalyst precursor, [Cp*RhCl$_2$]$_2$.[48] This shift clearly demonstrates a change in the coordination environment of the Rh cation and confirms the effective coordination by bpyCTF.

Optimization of the reaction conditions

Having successfully prepared Rh@bpyCTF, the heterogeneous catalyst was investigated for its catalytic performance in the transfer hydrogenation of N-heteroarenes using an aqueous buffer solution of formic acid and sodium formate as the hydrogen source. We initially focused on the reduction of quinoxaline derivatives and therefore used 2-methylquinoxaline **2a** as the model substrate to screen for the optimal reaction conditions. It should be noted that all reactions

were conducted without protective atmosphere and degassing, rendering the reduction more practical. Previous studies on the catalytic transfer hydrogenation of ketones, imines and N-heteroarenes in water demonstrated that the pH value of the medium has a critical effect on the reaction rate, with acidic conditions being more favorable.[21,23,36,49,50] We therefore investigated the activity of Rh@bpyCTF at various pH values ranging from 2.0 to 6.0 by altering the ratio of formic acid to sodium formate. As expected, high catalytic activities were observed only within a certain acidic pH window, with the highest conversion achieved at pH 4.5 (Figure 3a). This pH optimum is in agreement with that reported for the homogeneous [Cp*Rh(bpy)Cl]Cl complex, showing that immobilization on bpyCTF did not affect its pH dependency in the reaction.[36] Moreover, below pH 4, concomitant N-formylation of the formed hydrogenated product took place, which became more pronounced as the pH decreased. This side reaction is commonly observed when formic acid is used as the hydrogen donor and requires an additional hydrolysis step to convert the *N*-formyl side product into the desired product.[18] The effect of an excess of formate used in the reaction was then investigated (Figure 3b). As expected, the conversion rate increased rapidly with increasing concentrations of hydrogen donor. This acceleration leveled off when 40 equivalents of formate (4 M solution) were employed, and almost complete conversion was already obtained with 20 equivalents (2 M solution) after 2 h reaction. Therefore, 20 equivalents of formate were considered as an optimal amount. Temperature also had a pronounced effect on the transfer hydrogenation catalyzed by Rh@bpyCTF, with higher temperatures being more beneficial (Figure 3c). While a high conversion was achieved at 80 °C, the reaction rate decreased drastically when the reaction was carried out at room temperature, with only 4% conversion in 2 h. Even at an elevated temperature of 40 °C, the reaction proceeded slowly, reaching only 10% conversion. The catalyst loadings were then lowered to assess the effectiveness of the catalyst. As a control experiment, it was verified that the transfer hydrogenation of
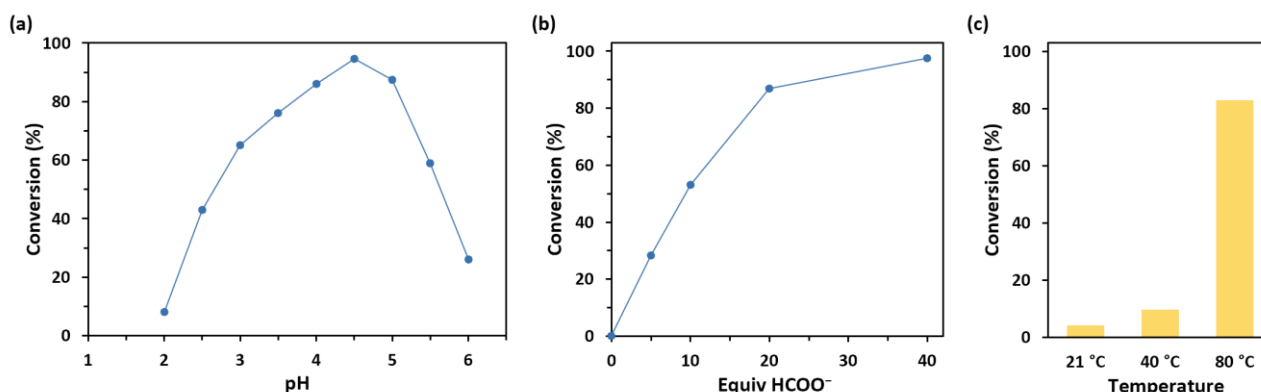
Figure 3. (a) Conversion as function of the medium's initial pH value. Reaction conditions: 2-methylquinoxaline **2a** (0.5 mmol), Rh@bpyCTF (0.25 mol% Rh), aqueous HCOOH/HCOONa buffer solution (2 M, 5 mL), 80 °C. Conversions were determined by ^{1}H NMR analysis after 20 min reaction. (b) Conversion as function of added equivalents formate. Reaction conditions: 2-mehtylquinoxaline **2a** (0.5 mmol), Rb@bpyCTF (0.25 mol% Rh), HCOOH/HCOONa buffer solution (resp. 0, 0.5, 1, 2, 4 M; pH 4.5, 5 mL), 80 °C. Conversions were determined by ^{1}H NMR analysis after 2 h reaction. (c) Temperature effect on the transfer hydrogenation reaction rate of 2-methylquinoxaline **2a** (0.5 mmol) catalyzed by Rh@bpyCTF in a HCOOH/HCOONa buffer solution (2 M, pH 4.5, 5 mL). Conversions were determined by ^{1}H NMR analysis after 2 h reaction.

Table 1. Rhodium-catalyzed transfer hydrogenation of 2-methylquinoxaline.[a]

| Entry	Catalyst	Rh (mol%)	Time (h)	Conversion (%)[b]
1	none	–	24	0
2	bpyCTF	–	24	0
3	Rh@bpyCTF	0.25	2	>99
4[c]	Rh@bpyCTF	0.1	2	36
5[c]	Rh@bpyCTF	0.1	24	90
6[d]	Rh@bpyCTF	0.02	24	28
7	[Cp*RhCl$_2$]$_2$	0.25	24	0
8	[Cp*Rh(bpy)Cl]Cl	0.25	1	98

[a] Reaction conditions: 2-methylquinoxaline **2a** (0.5 mmol), Rh complex or Rh@bpyCTF (0.25 mol% Rh, 5.6 mg Rh@bpyCTF), aqueous HCOOH/HCOONa buffer (2 M, pH 4.5, 5 mL), 80 °C. [b] Determined by ^{1}H NMR analysis. [c] 1.25 mmol of **2a** in 12.5 mL buffer solution. [d] 6.25 mmol of **2a** in 62.5 mL buffer solution.

2-methylquinoxaline **2a** did not take place in absence of the Rh catalyst (Table 1, entry 1). Similarly, pristine bpyCTF itself did not show any activity. In contrast, the reaction with Rh@bpyCTF was completed in 2 h with a catalyst loading of 0.25 mol% Rh (entry 2). Reducing the loading to 0.1 mol% Rh gave a conversion of 36% after the same reaction time, but increased to 90% after 24 h (entries 4 and 5). Further reducing the loading to 0.02 mol% Rh resulted in a conversion of only 28% after 24 h (entry 6). The catalyst precursor, [Cp*RhCl$_2$]$_2$, showed no activity, while the homogeneous [Cp*Rh(bpy)Cl]Cl catalyst gave almost complete conversion in 1 h (entries 7 and 8).

The kinetic profiles of the transfer hydrogenation reaction under the homogeneous and heterogeneous catalysis are compared in Figure 4. In both cases, the hydrogen transfer is fast from the beginning. The rate of the heterogeneous reaction was slightly lower than that of the homogeneous counterpart, due to diffusion limitations inherent to a porous matrix such as bpyCTF.

Hot-filtration test

The heterogeneity of the Rh@bpyCTF catalyst was assessed through a hot-filtration test. To this end, Rh@bpyCTF was removed from the reaction mixture by filtration partway through the transfer hydrogenation reaction. The filtrate was then allowed to react further for an additional 18 h. Once the
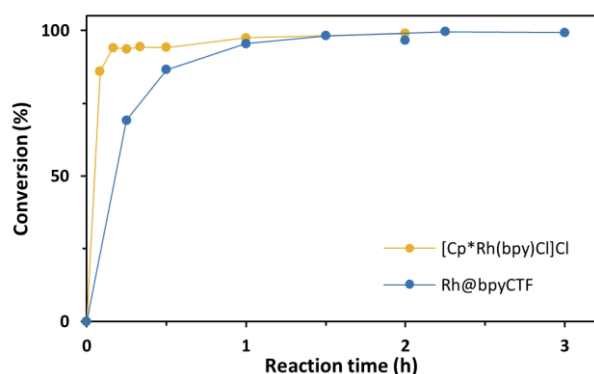
Figure 4. Reaction profiles for the transfer hydrogenation catalyzed by heterogeneous Rh@bpyCTF compared to homogeneous [Cp*Rh(bpy)Cl]Cl. Reaction conditions: 2-methylquinoxaline **2a** (0.5 mmol), Rh catalyst (0.25 mol% Rh), aqueous HCOOH/HCOONa buffer solution (2 M, pH 4.5, 5 mL) at 80 °C.
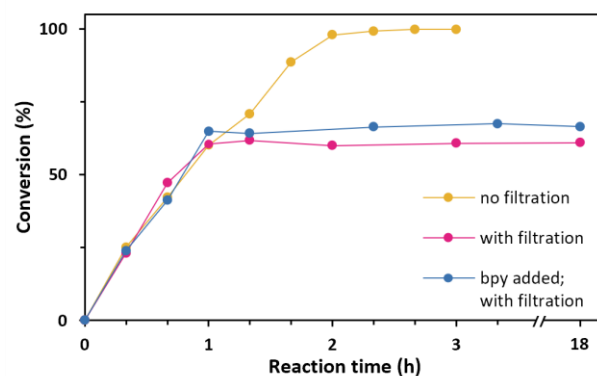
Figure 5. Hot-filtration test for Rh@bpyCTF. Yellow: unfiltered reaction with 2-methylquinoxaline **2a** (0.5 mmol), Rh@bpyCTF (5.6 mg, 0.25 mol% Rh), aqueous HCOOH/HCOONa solution (2 M, pH 4.5, 5 mL), 80 °C. Pink: the catalyst was removed by filtration after 1 h. Blue: 2,2'-bipyridine (1.25 mol%) was added from the start of the reaction. The catalyst was removed by filtration after 1 h.

catalyst was removed, no further conversion of the substrate was observed, showing that the catalysis is truly performed by the heterogeneous Rh@bpyCTF, and that leaching of the active metal species is negligible (Figure 5). However, since potentially leached Cp*Rh species might not be active for the transfer hydrogenation without comprising a 2,2'-bipyridine ligand (cf. Table 1, entry 7), an additional filtration test was performed in which free bipyridine ligand was added to the reaction mixture from the start. Again, no increase in substrate conversion was observed, demonstrating that bpyCTF firmly coordinates the Rh complex.

Substrate scope

Considering the good performance of Rh@bpyCTF under the optimized conditions, the general applicability of the catalyst was studied by the transfer hydrogenation of various quinoxalines and, by extension, of other N-heteroaromatic scaffolds. *In concreto*, a wide range of 2- and 2,3-substituted quinoxaline substrates **2a–g** with small and bulky substituents and quinoxalines with electron-donating and -withdrawing groups on the C6-position **2h–k** was reacted to give the corresponding 1,2,3,4-tetrahydroquinoxalines **3a–j** in good to excellent yields (75–96%). The reactions were carried out using an aqueous HCOOH/HCOONa buffer solution at the optimal pH 4.5 and at 80 °C. From the initial attempts it became clear that some of the quinoxaline substrates required prolonged reaction times. To ensure the buffering capability of the reaction solution, the buffer solution of 2 M was increased to a 4 M HCOOH/HCOONa buffer solution. Moreover, in the process of studying the substrate scope we found that not all the substrates dissolved well in the aqueous medium, which may lead to low conversions. Therefore, substrates were introduced into the reaction mixture as a concentrated solution in EtOAc. Rh@bpyCTF exhibited high reactivity toward all the quinoxalines examined, with full conversions within 10 h or less, using a low catalyst loading of 0.25 mol% Rh (Table 2). The 2-substitued quinoxalines **2b** and **2c**, bearing a sterically demanding *tert*-butyl and phenyl group, respectively, were

smoothly hydrogenated to the corresponding tetrahydroquinoxalines, albeit with prolonged reaction times. The reactions with 2,3-dialkyl-substitued quinoxalines **2d,e,h–j** afforded the corresponding tetrahydroquinoxalines as mixtures of *cis*- and *trans*-isomers, with the *cis*-isomer predominating. The diastereoselectivity for tetrahydroquinoxalines **3d,e,h–j** could be determined based on the chemical shifts and coupling constants (*J*) of the C2 and C3 methine protons in ^{1}H NMR spectroscopy ($\delta_{H,trans} < \delta_{H,cis}$ and $J_{H2-H3,cis} < J_{H2-H3,trans}$).[51] In contrast, only one diastereomer was observed when quinoxalines **2f** and **2g**, which both feature a phenyl group on the pyrazine ring, were employed in the reaction. The relative configuration of tetrahydroquinoxaline **3f** could be easily deduced from the ^{1}H NMR spectrum (CDCl$_3$), showing a small vicinal coupling constant of 3.2 Hz between the C2 and C3 methine protons that is consistent with substituents adopting the *cis*-configuration.[52] In the case of tetrahydroquinoxaline **3g**, the ^{1}H NMR signal (CDCl$_3$) of the methine protons appeared as a singlet at 4.74 ppm, which agrees with the chemical shift reported for the *cis*-isomer.[52] In addition, single-crystal X-ray diffraction analysis of **3g** unequivocally established the *cis*-configuration of the phenyl substituents (Figure 6). Furthermore, the Rh@bpyCTF-catalyzed reaction was compatible with the electron-donating methoxy group (entry 8), and with the electron-withdrawing cyano and halogen substituents (entries 9 and 10). Quinoxalines **2h–j** were readily transformed and the corresponding tetrahydroquinoxalines **3h–j** were isolated in excellent yields. Fortunately, no dehalogenation was observed in the case of the chlorine substituted quinoxaline **2i**. Accelerated hydrogen transfer was noticed for quinoxaline **2j** because the electron-withdrawing cyano group renders the substrate more susceptible for nucleophilic attack. For 6-nitro-2,3-dimethylquinoxaline **2k**, the aromaticity of the quinoxaline scaffold was retained under these conditions, while the nitro group was chemoselectively reduced to an amino group, yielding 2,3-dimethylquinoxalin-6-amine **2k** in a yield of 77%.

Following the successful transformation of these quinoxaline derivatives, the potential of Rh@bpyCTF as a versatile catalyst was further demonstrated by extending the scope to various other N-heteroaromatic scaffolds (Table 3). Under the same reaction conditions, all of the examined N-heteroarenes were reduced with full conversion, and the corresponding products could be isolated in very good to excellent yields (80–99%).
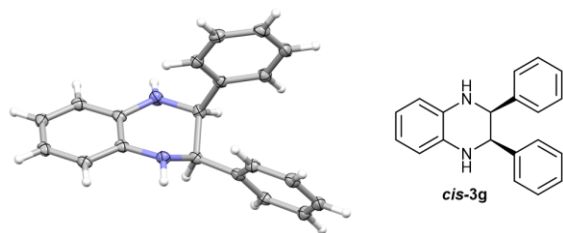
Figure 6. Molecular structure of *meso*-2,3-diphenyl-1,2,3,4-tetrahydroquinoxaline **3g**, showing the *cis*-configuration of the phenyl substituents. Thermal displacement ellipsoids are drawn at the 50% probability level. (CCDC 2226036)
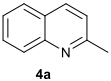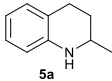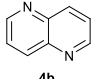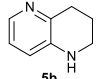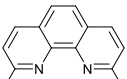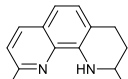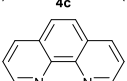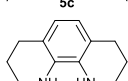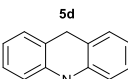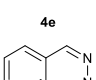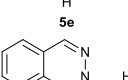
Table 2. Transfer hydrogenation of quinoxalines in water catalyzed by Rh@bpyCTF.[a]

Entry	Substrate	Product	Time (h)	Yield (%)[b]
1	**2a**	**3a**	3	94
2	**2b**	**3b**	9	80
3	**2c**	**3c**	10	85
4	**2d**	**3d**	5	76 (75/25)[c]
5	**2e**	**3e**	5	82 (83/17)[c]
6	**2f**	*cis*-**3f**	8	75 (100/0)[c]
7	**2g**	*cis*-**3g**	10	77 (100/0)[c]
8	**2h**	**3h**	8	95 (74/26)[c]
9	**2i**	**3i**	7	92 (81/19)[c]
10	**2j**	**3j**	2	96 (83/17)[c]
11	**2k**	**3k**	8	77

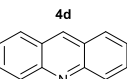[a] Reaction conditions: substrate **2** (0.7 mmol), Rh@bpyCTF (0.25 mol% Rh), HCOOH/HCOONa (4 M, pH 4.5, 7 mL), 80 °C. Substrates were added as a concentrated solution in EtOAc (1 M). [b] Isolated yields. [c] *Cis/trans* ratio determined by ^{1}H NMR analysis (CDCl$_3$) of the crude reaction mixture.

2-Methylquinoline **4a** was reduced in a clean and regioselective reaction, yielding 2-methyl-1,2,3,4-tetrahydroquinoline **5a** in very high purity and nearly quantitative yield (99%). 1,5-Naphthyridine **4b** was selectively hydrogenated in only one pyridine ring. The reaction with phenanthrolines **4c** and **4d**, both strong N-bidentate ligands, did not hamper the activity of Rh@bpyCTF (entries 3 and 4).

Table 3. Transfer hydrogenation of various N-heteroaromatic scaffolds in water catalyzed by Rh@bpyCTF.[a]

Entry	Substrate	Product	Time (h)	Yield (%)[b]
1	4a	5a	4	99
2	4b	5b	8	85
3	4c	5c	6	87
4	4d	5d	24	82
5	4e	5e	1	91
6	4f	5f	24	80

[a] Reaction conditions: Substrate **4** (0.7 mmol), Rh@bpyCTF (0.25 mol% Rh), aqueous HCOOH/HCOONa (4 M, pH 4.5, 7 mL), 80 °C. Substrates were added as a concentrated solution in EtOAc (1 M). [b] Isolated yields.

The reduction of 2,9-dimethyl-1,10-phenanthroline **4c** gave the partially hydrogenated 1,2,3,4-tetrahydrophenanthroline **5c** as the sole product, which is in line with findings in previous reports.[53] In sharp contrast, the reduction of unsubstituted 1,10-phenanthroline attained complete conversion in 3 h, but resulted in a mixture of tetrahydrophenanthroline and octahydrophenanthroline **5d** (THphen/OHphen = 73/27). Upon extending the reaction time to 24 h, complete conversion to the latter compound was achieved. Furthermore, acridine **4e** was readily reduced to the 9,10-dihydro product **5e** and obtained in a high yield of 91%. In the reduction of phthalazine **4f** only one of the imine bonds was hydrogenated, while the other imine bond remained untouched. Moreover, the hydrogenated product underwent fast N-formylation at the amino nitrogen, and complete conversion to phthalazine-2(1*H*)-carbaldehyde **5f** was obtained. The *N*-formyl group of phthalazine-2(1*H*)-carbaldehyde **5f** could be cleaved by NaOH-mediated hydrolysis in an ethanol/water mixture under reflux conditions (Scheme S1, ESI). However, the targeted 1,2-dihydrophthalazine **6** could not be isolated in a pure state. ^{1}H NMR analysis revealed that the crude product also comprised phthalazine **4f** to a minor extent (**6/4f** = 96/4). A second ^{1}H NMR analysis of the same sample four days later showed an increase in the portion of phthalazine (**6/4f** = 79/21), indicating that 1,2-dihydrophthalazine **6** is sensitive to air and was readily oxidized upon exposure during the hydrolysis reaction. This finding agrees with reports in the literature.[54,55] Nonetheless, a straightforward procedure is provided for the cleavage of the *N*-formyl group, which can be extrapolated to other N-heterocycles.
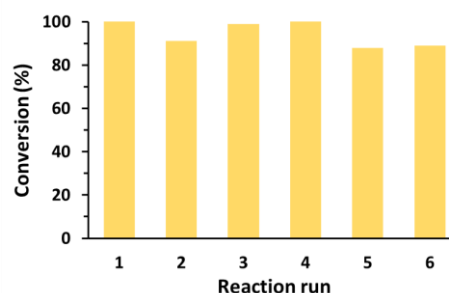

Figure 7. Reusability experiment with Rh@bpyCTF. Conversions toward **3a** were determined by ^{1}H NMR analysis after 3 h reaction. The lower conversion in the 2nd reaction run is most likely due to batch variability. Reaction conditions: **2a** (2.5 mmol), Rh@bpyCTF (28.1 mg, 0.25 mol% Rh), aqueous HCOOH/HCOONa solution (4 M, pH 4.5, 25 mL), 80 °C, 3 h.

Catalyst recycling experiments

To be relevant in practical applications, the catalyst must maintain its high activity during several reaction runs. Hence, the long-term stability was investigated over six runs. After each run the catalyst was recovered by filtration and dried at 100 °C before being reused in the next reaction. In general, the catalyst maintained high activity throughout the recycling experiment, demonstrating its high stability (Figure 7). However, in the 5th run the conversion toward **3a** slightly decreased to 89%, yet complete conversion was achieved upon prolonged reaction times. In the 6th run, the conversion remained steady and did not decrease further. Furthermore, the crude product obtained in the first run did not contain any detectable amount of leached rhodium (< 0.003 wt%) as evidenced by ICP-OES analysis. Moreover, the Rh loading on Rh@bpyCTF after six reaction runs was still 1.9 wt%. XPS analysis of Rh@bpyCTF after recycling showed no change in the binding state of the Rh metal center (Figure S6, ESI).

Catalyst comparison

To demonstrate the merit of our catalytic system, we compared the Rh@bpyCTF-catalyzed transfer hydrogenation to other reported heterogeneous catalytic systems that use formic acid or formate as the hydrogen source (Table 4). Although a one-on-one comparison is not straightforward because of the different reaction conditions, the comparison of the catalysts showed that Rh@bpyCTF is a very efficient catalyst, achieving high reaction rates with a lower catalyst loading, and can operate effectively in water as a green solvent (entries 1 and 2 vs. 7).[56] Besides, no protective atmosphere was required, adding to the operational simplicity of the reaction (entry 5 vs. 7). Moreover, by controlling the pH, we were able to selectively reduce the substrate to the non-formylated product, whereas the catalytic systems of entries 1 and 6 yielded mixtures that thus required an additional hydrolysis step. Rh@bpy-PMO of Matsui *et al.* showed similar high activity as Rh@bpyCTF, but lost significant activity after four reaction runs (entry 3).[57]

Table 4. Comparison of Rh@bpyCTF to reported heterogeneous catalysts for the transfer hydrogenation of 2-methylquinoline with formic acid or formate.

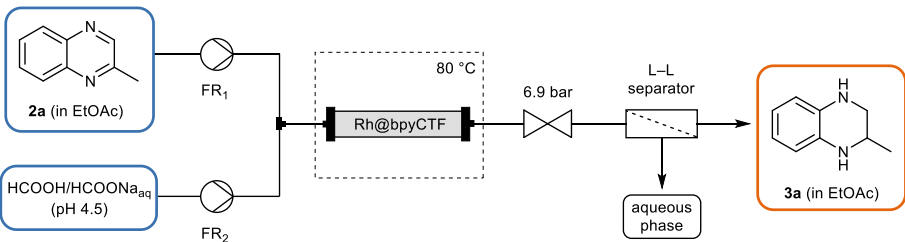| Entry	Catalyst	Catalyst loading	Conditions	TON[a]	TOF (h^{-1})[b]	Ref.
1	Au@NH$_2$-SBA-15	1 mol% Au	HCOOH (30 eq), Et$_3$N (5.25 eq), anh. DMF, 130 °C	100	31.7	58
2	Au/TiO$_2$-R	1 mol% Au	HCOOH (20 eq), Et$_3$N/DMF (1/8), 130 °C	99	235	59
3	Rh@bpy-PMO	0.2 mol% Rh	HCOOH/HCOONa (8.7 eq), H$_2$O, 80 °C	500[c]	120	57
4	Ir/Si	1 mol% Ir	HCOOH (2 eq), H$_2$O, 80 °C	100	7.3	60
5	Co@OMNC-700	10.6 mol% Co	HCOOH (8.5 eq), H$_2$O, N$_2$ atm, 140 °C	9.4[d]	2.3	61
6	Co@C-N$_{800}$	0.9 mol% Co	HCOOH (15 eq), H$_2$O, 130 °C	100[d,e]	16.8	62
7	Rh@bpyCTF	0.25 mol% Rh	HCOOH/HCOONa (40 eq), H$_2$O, 80 °C	400	100	This work

[a] Turnover number. [b] Global turnover frequency over the course of the reaction. [c] 2,3-Dimethylquinoxaline as substrate. [d] Quinoline as substrate. [e] Also N-formylated product, 87% selectivity.

Continuous flow transfer hydrogenation

Given the good performance of Rh@bpyCTF under batch conditions, we wanted to take full advantage of the heterogenization of the Rh catalyst and translated the batch transfer hydrogenation reaction into a continuous flow process using microreactor technology. Immobilizing the CTF-supported Rh complex in a packed-bed column results in a high local concentration of the Rh catalyst, which could lead to higher reaction rates. Moreover, separation of the catalyst from the product is inherent since the catalyst is retained in the column. Although catalytic transformations under flow conditions are receiving increased attention, the use of COFs as catalysts in liquid flow reactions is still in its infancy, as is reflected in the scarce number of reported studies.[63,64]

To explore the feasibility of Rh@bpyCTF being applied in a continuous flow process, proof-of-concept experiments were conducted on the transfer hydrogenation of 2-methylquinoxaline. A packed-bed reactor was prepared by filling a PTFE tubing with a mixture of Rh@bpyCTF and glass beads (Figure S8, ESI). The inert glass beads were added to overcome high back pressures due to the accommodation of fine particles. The packed-bed column was heated to 80 °C by means of a GC oven and reagents were passed through the column by means of reciprocating pumps. A liquid–liquid separator (Zaiput) was integrated at the end of the setup to separate the organic product stream from the aqueous formate stream. The conversions toward the product **3a** obtained by varying the conditions are summarized in Table 5. Nearly complete conversion of **2a** was achieved in short contact times by using large excess of formate (entry 1). However, the high conversion could not be maintained for long periods of time due to channel formation and moving of the CTF particles inside the packed bed. Therefore, a more robust reactor design is proposed in which the packed bed consist of smaller consecutive segments of CTF (Figure S9, ESI).

Table 5. Preliminary results of the continuous flow transfer hydrogenation with a Rh@bpyCTF-catalyst bed.

Entry[a]	[2a] (M)	[HCOO$^-$] (M)	FR$_1$ (mL min^{-1})	FR$_2$ (mL min^{-1})	HCOO$^-$ (eq)	CT[b] (s)	TOS[c] (min)	Conversion[d] (%)
1	0.5	2	0.1	0.9	36	20	20	97
							25	94
2	0.25	0.5	0.2	0.8	8	20	15	58
							20	58
							25	41
3	0.25	1	0.2	0.8	16	20	15	74
							20	68
							25	62
4	0.5	2	0.1	0.4	16	40	15	99
							20	84
							25	59

[a] Experiments were performed in the given order using the same packed-bed column. [b] Approximated mean contact time of the reactants with the catalyst bed. [c] Time-on-stream. [d] Determined by ^{1}H NMR analysis. (FR = flow rate)

Conclusions

In summary, a bipyridine-based CTF has been successfully applied as support for the immobilization of a Cp*Rh(III) complex. The heterogeneous Rh@bpyCTF catalyst exhibited high activity for the transfer hydrogenation of N-heteroarenes in water, using easy-to-handle sodium formate as the hydrogen donor. The reactivity was highly pH dependent, with the highest conversion rate at pH 4.5. A very wide range of quinoxalines and other N-heteroarenes underwent transfer hydrogenation to afford the products in good to excellent yields, highlighting the versatility of the catalyst. Moreover, the catalyst could be easily recovered by filtration and the recovered catalyst remained highly active for at least six reaction runs, proving the sustainable nature of this catalytic system. Additionally, the applicability of the catalyst under continuous flow conditions was explored in preliminary experiments, but the reactor design needs further optimization. All together, bpyCTF performed well as a support material for the heterogenization of molecular metal complexes, hereby bridging the gap between homogeneous and heterogeneous catalysis.

Author Contributions

Conceptualization: JE, CS; investigation: JE; funding acquisition: JE, VVS, PVDV, CS; supervision: VVS, PVDV, CS; writing – original draft: JE; writing – review & editing: JE, KL, MD, KVH, PVDV, CS. HR performed the STEM-EDX analyses; KL performed the XPS analyses under the supervision of RM and NDG; MD contributed to the characterization of the catalyst; KVH performed the single-crystal X-ray diffraction analysis.

Conflicts of interest

There are no conflicts to declare.

Acknowledgements

Notes and references

1   S. G. Davies, A. M. Fletcher, P. M. Roberts and J. E. Thomson, *Eur. J. Org. Chem.*, 2019, **2019**, 5093–5119.
2   Y. Matsumoto, R. Tsuzuki, A. Matsuhisa, T. Yoden, Y. Yamagiwa, I. Yanagisawa, T. Shibanuma and H. Nohira, *Biorg. Med. Chem.*, 2000, **8**, 393–404.
3   C. T. Eary, Z. S. Jones, R. D. Groneberg, L. E. Burgess, D. A. Mareska, M. D. Drew, J. F. Blake, E. R. Laird, D. Balachari, M. O'Sullivan, A. Allen and V. Marsh, *Biorg. Med. Chem. Lett.*, 2007, **17**, 2608–2613.
4   E. Vitaku, D. T. Smith and J. T. Njardarson, *J. Med. Chem.*, 2014, **57**, 10257–10274.
5   R. P. Law, S. J. Atkinson, P. Bamborough, C.-w. Chung, E. H. Demont, L. J. Gordon, M. Lindon, R. K. Prinjha, A. J. B. Watson and D. J. Hirst, *J. Med. Chem.*, 2018, **61**, 4317–4334.
6   H.-X. Lei, K. Zhang, Y.-X. Qin, R.-J. Dong, D.-Z. Chen, H. Zhou and X.-H. Sheng, *J. Mol. Struct.*, 2021, **1228**, 129485.
7   D. Cao, J. Yu, H. Wang, Z. Luo, X. Liu, L. He, J. Qi, L. Fan, L. Tang, Z. Chen, J. Li, J. Cheng and S. Wang, *Science*, 2022, **375**, 403–411.
8   X. Zhang, H. Xu, H. Su, X. Yang, T. Sun, X. Lu, F. Shi, H. Duan, X. Liu and Y. Ling, *J. Agric. Food. Chem.*, 2022, **70**, 1776–1787.
9   F. Lovering, J. Bikker and C. Humblet, *J. Med. Chem.*, 2009, **52**, 6752–6756.
10   M. Aldeghi, S. Malhotra, D. L. Selwood and A. W. E. Chan, *Chem. Biol. Drug Des.*, 2014, **83**, 450–461.
11   Y.-G. Zhou, *Acc. Chem. Res.*, 2007, **40**, 1357–1366.
12   D.-S. Wang, Q.-A. Chen, S.-M. Lu and Y.-G. Zhou, *Chem. Rev.*, 2012, **112**, 2557–2590.
13   R. Gunasekar, R. L. Goodyear, I. Proietti Silvestri and J. Xiao, *Org. Biomol. Chem.*, 2022, **20**, 1794–1827.
14   D. Wang and D. Astruc, *Chem. Rev.*, 2015, **115**, 6621–6686.
15   R. Nie, Y. Tao, Y. Nie, T. Lu, J. Wang, Y. Zhang, X. Lu and C. C. Xu, *ACS Catal.*, 2021, **11**, 1071–1095.
16   A. Robertson, T. Matsumoto and S. Ogo, *Dalton Trans.*, 2011, **40**, 10304–10310.
17   Y. Wei, X. Wu, C. Wang and J. Xiao, *Catal. Today*, 2015, **247**, 104–116.
18   D. Talwar, H. Y. Li, E. Durham and J. Xiao, *Chem. Eur. J.*, 2015, **21**, 5370–5379.
19   J. Fidalgo, M. Ruiz-Castañeda, G. García-Herbosa, A. Carbayo, F. A. Jalón, A. M. Rodríguez, B. R. Manzano and G. Espino, *Inorg. Chem.*, 2018, **57**, 14186–14198.
20   X. Wu, X. Li, W. Hems, F. King and J. Xiao, *Org. Biomol. Chem.*, 2004, **2**, 1818–1821.
21   X. Wu, X. Li, F. King and J. Xiao, *Angew. Chem. Int. Ed.*, 2005, **44**, 3407–3411.
22   X. Wu, X. Li, A. Zanotti-Gerosa, A. Pettman, J. Liu, A. J. Mills and J. Xiao, *Chem. Eur. J.*, 2008, **14**, 2209–2222.
23   Q. Lei, Y. Wei, D. Talwar, C. Wang, D. Xue and J. Xiao, *Chem. Eur. J.*, 2013, **19**, 4021–4029.
24   J. Artz, *ChemCatChem*, 2018, **10**, 1753–1771.
25   M. Liu, L. Guo, S. Jin and B. Tan, *J. Mater. Chem. A*, 2019, **7**, 5153–5172.
26   C. Krishnaraj, H. S. Jena, K. Leus and P. Van Der Voort, *Green Chem.*, 2020, **22**, 1038–1071.
27   A. Iemhoff, M. Vennewald and R. Palkovits, *Angew. Chem. Int. Ed.*, 2023, **62**, e202212015.
28   P. Kuhn, A. Forget, D. Su, A. Thomas and M. Antonietti, *J. Am. Chem. Soc.*, 2008, **130**, 13333–13337.
29   R. Palkovits, M. Antonietti, P. Kuhn, A. Thomas and F. Schüth, *Angew. Chem. Int. Ed.*, 2009, **48**, 6909–6912.
30   S. Hug, M. E. Tauchert, S. Li, U. E. Pachmayr and B. V. Lotsch, *J. Mater. Chem.*, 2012, **22**, 13956–13964.
31   S. Rajendiran, P. Natarajan and S. Yoon, *RSC Adv.*, 2017, **7**, 4635–4638.

32 N. Tahir, F. Muniz-Miranda, J. Everaert, P. Tack, T. Heugebaert, K. Leus, L. Vincze, C. V. Stevens, V. Van Speybroeck and P. Van der Voort, *J. Catal.*, 2019, **371**, 135–143.

33 S. Abednatanzi, P. G. Derakhshandeh, P. Tack, F. Muniz-Miranda, Y. Y. Liu, J. Everaert, M. Meledina, F. Vanden Bussche, L. Vincze, C. V. Stevens, V. Van Speybroeck, H. Vrielinck, F. Callens, K. Leus and P. Van Der Voort, *Appl. Catal. B Environ.*, 2020, **269**.

34 K. Park, G. H. Gunasekar, S.-H. Kim, H. Park, S. Kim, K. Park, K.-D. Jung and S. Yoon, *Green Chem.*, 2020, **22**, 1639–1649.

35 P. Sudakar, G. H. Gunasekar, I. H. Baek and S. Yoon, *Green Chem.*, 2016, **18**, 6456–6461.

36 L. Zhang, R. Qiu, X. Xue, Y. Pan, C. Xu, H. Li and L. Xu, *Adv. Synth. Catal.*, 2015, **357**, 3529–3537.

37 L.-Y. Liao, X.-R. Kong and X.-F. Duan, *J. Org. Chem.*, 2014, **79**, 777–782.

38 J. Everaert, M. Debruyne, F. Vanden Bussche, K. Van Hecke, T. S. A. Heugebaert, P. Van Der Voort, V. Van Speybroeck and C. V. Stevens, *Synthesis*, 2023, **55**, 333–340.

39 P. Kuhn, M. Antonietti and A. Thomas, *Angew. Chem. Int. Ed.*, 2008, **47**, 3450–3453.

40 D. Y. Osadchii, A. I. Olivos-Suarez, A. V. Bavykina and J. Gascon, *Langmuir*, 2017, **33**, 14278–14285.

41 M. Thommes, K. Kaneko, A. V. Neimark, J. P. Olivier, F. Rodriguez-Reinoso, J. Rouquerol and K. S. W. Sing, *Pure Appl. Chem.*, 2015, **87**, 1051–1069.

42 S. Hug, L. Stegbauer, H. Oh, M. Hirscher and B. V. Lotsch, *Chem. Mater.*, 2015, **27**, 8001–8010.

43 M. Ayiania, M. Smith, A. J. R. Hensley, L. Scudiero, J.-S. McEwen and M. Garcia-Perez, *Carbon*, 2020, **162**, 528–544.

44 K. Stańczyk, R. Dziembaj, Z. Piwowarska and S. Witkowski, *Carbon*, 1995, **33**, 1383–1392.

45 K. Artyushkova, *J. Vac. Sci. Technol. A*, 2020, **38**, 031002.

46 M. Soorholtz, L. C. Jones, D. Samuelis, C. Weidenthaler, R. J. White, M.-M. Titirici, D. A. Cullen, T. Zimmermann, M. Antonietti, J. Maier, R. Palkovits, B. F. Chmelka and F. Schüth, *ACS Catal.*, 2016, **6**, 2332–2340.

47 F. M. Wisser, P. Berruyer, L. Cardenas, Y. Mohr, E. A. Quadrelli, A. Lesage, D. Farrusseng and J. Canivet, *ACS Catal.*, 2018, **8**, 1653–1661.

48 Y. Hayashi, K. Toriumi and K. Isobe, *J. Am. Chem. Soc.*, 1988, **110**, 3666–3668.

49 S. Ogo, T. Abura and Y. Watanabe, *Organometallics*, 2002, **21**, 2964–2969.

50 C. Wang, C. Li, X. Wu, A. Pettman and J. Xiao, *Angew. Chem. Int. Ed.*, 2009, **48**, 6524–6528.

51 R. A. Archer and H. S. Mosher, *J. Org. Chem.*, 1967, **32**, 1378–1381.

52 Z. Zhang and H. Du, *Angew. Chem. Int. Ed.*, 2015, **54**, 623–626.

53 L. Wang, J. Lin, C. Xia and W. Sun, *J. Org. Chem.*, 2021, **86**, 16641–16651.

54 A. Hisrch and D. G. Orphanos, *J. Heterocycl. Chem.*, 1966, **3**, 38–41.

55 C.-K. Sha and C.-P. Tsou, *J. Chin. Chem. Soc.*, 1991, **38**, 183–186.

56 D. Prat, A. Wells, J. Hayler, H. Sneddon, C. R. McElroy, S. Abou-Shehada and P. J. Dunn, *Green Chem.*, 2016, **18**, 288–296.

57 K. Matsui, Y. Maegawa, M. Waki, S. Inagaki and Y. Yamamoto, *Catal. Sci. Technol.*, 2018, **8**, 534–539.

58 B. Vilhanová, J. A. van Bokhoven and M. Ranocchiari, *Adv. Synth. Catal.*, 2017, **359**, 677–686.

59 L. Tao, Q. Zhang, S.-S. Li, X. Liu, Y.-M. Liu and Y. Cao, *Adv. Synth. Catal.*, 2015, **357**, 753–760.

60 J.-F. Zhang, R. Zhong, Q. Zhou, X. Hong, S. Huang, H.-Z. Cui and X.-F. Hou, *ChemCatChem*, 2017, **9**, 2496–2505.

61 G. Li, H. Yang, H. Zhang, Z. Qi, M. Chen, W. Hu, L. Tian, R. Nie and W. Huang, *ACS Catal.*, 2018, **8**, 8396–8405.

62 A. K. Kar and R. Srivastava, *ACS Sustain. Chem. Eng.*, 2019, **7**, 13136–13147.

63 R. S. B. Gonçalves, A. B. V. de Oliveira, H. C. Sindra, B. S. Archanjo, M. E. Mendoza, L. S. A. Carneiro, C. D. Buarque and P. M. Esteves, *ChemCatChem*, 2016, **8**, 743–750.

64 N. Wang, F. Wang, F. Pan, S. Yu and D. Pan, *ACS Appl. Mater. Interfaces*, 2021, **13**, 3209–3220.